NASA
Technical Memorandum 83578

AVRADCOM
Technical Report 84-C-2

Hydrodynamic Lubrication of Rigid Nonconformal Contacts in Combined Rolling and Normal Motion

Mihir K. Ghosh and Bernard J. Hamrock
Lewis Research Center
Cleveland, Ohio

and

David E. Brewe
Propulsion Laboratory
AVRADCOM Research and Technology Laboratories
Lewis Research Center
Cleveland, Ohio

Prepared for the
Joint Lubrication Conference
cosponsored by the American Society of Mechanical Engineers
and the American Society of Lubrication Engineers
San Diego, California, October 22-24, 1984

NASA

HYDRODYNAMIC LUBRICATION OF RIGID NONCONFORMAL CONTACTS IN COMBINED ROLLING AND NORMAL MOTION

M. K. Ghosh* and Bernard J. Hamrock
National Aeronautics and Space Administration
Lewis Research Center
Cleveland, Ohio

and

David E. Brewe
Propulsion Laboratory
AVRADCOM Research and Technology Laboratories
Lewis Research Center
Cleveland, Ohio

ABSTRACT

A numerical solution to the problem of hydrodynamic lubrication of rigid point contacts with an isoviscous, incompressible lubricant has been obtained. The hydrodynamic load-carrying capacity under unsteady (or dynamic) conditions arising from the combined effects of squeeze motion superposed upon the entraining motion has been determined for both normal approach and separation. Superposed normal motion considerably increases net load-carrying capacity during normal approach and substantially reduces net load-carrying capacity during separation. Geometry has also been found to have a significant influence on the dynamic load-carrying capacity. The ratio of dynamic to steady state load-carrying capacity increases with increasing geometry parameter for normal approach and decreases during separation. The cavitation (film rupture) boundary is also influenced significantly by the normal motion, moving downstream during approach and upstream during separation. For sufficiently high normal separation velocity the rupture boundary may even move upstream of the minimum-film-thickness position.

E-1926

*Banaras Hindu University, Varanasi, India, and NRC-NASA Research Associate.

Sixty-three cases were used to derive a functional relationship for the ratio of the dynamic to steady state load-carrying capacity β in terms of the dimensionless normal velocity parameter q (incorporating normal velocity, entraining velocity, and film thickness) and the geometry parameter α. The result is expressed in the form

$$\beta = \left\{\alpha^{-0.028} \text{ sech } (1.68\ q)\right\}^{1/q}$$

The ratio of the dynamic to steady state peak pressures in the contact ξ increases considerably with increasing normal velocity parameter during normal approach, with a similar decrease during separation. The ratio is expressed as a function of q and α by

$$\xi = \left\{\alpha^{-0.032} \text{ sech } (2q)\right\}^{1/q}$$

NOMENCLATURE

a	Amplitude of harmonic motion, m
h	Film thickness, m
h_{in}	Fluid inlet level, m
h_0	Central (or minimum) film thickness, m
H	Dimensionless film thickness, h/R_x
H_{in}	Dimensionless fluid inlet level, h_{in}/R_x
H_0	Dimensionless minimum (or central) film thickness, h_0/R_x
p	Pressure, N/m^2
p_{max}	Maximum or peak pressure along line of minimum film thickness, N/m^2
P	Dimensionless pressure, $pR_x/\eta_0 U_S$
P_{max}	Dimensionless peak pressure along line of minimum film thickness, N/m^2
q	Dimensionless normal velocity parameter, $U_N/U_S\ (1/2\ H_0)^{1/2}$
R	Effective radius of curvature, $R_xR_y/(R_x + R_y)$, m
S	Separation due to geometry of solid, m
U_A, U_B	Surface velocity of solids A and B
U_N	Normal velocity of approach or separation of solids, m

$\bar{U}_N$	Dimensionless normal velocity, U_N/U_S
U_S	Average surface velocity, $(U_A + U_B)/2$, m
t	Time, sec
x	Coordinate along rolling direction, m
x_p	Location of peak pressure from minimum-film-thickness position, m
x_r	Location of film rupture boundary from minimum-film-thickness position, m
X	Dimensionless coordinate, x/R_x
X_p	Dimensionless location of peak pressure from minimum-film-thickness position on line of minimum film thickness, x_p/R_x
X_r	Dimensionless location of film rupture boundary from minimum-film-thickness position on line of minimum film thickness, x_r/R_x
y	Coordinate transverse to rolling direction, m
Y	Dimensionless coordinate, y/R_x
w	Load-carrying capacity, N
W	Dimensionless load-carrying capacity, $w/\eta_0 U_S R_x$
α	Radius ratio (geometry parameter), R_y/R_x
β	Dynamic load ratio (ratio of dimensionless dynamic to steady state load-carrying capacity), $W/(W)q = 0$
ϵ	Amplitude ratio, $a/(h_0)_{mean}$
η_0	Fluid viscosity at standard temperature and pressure, N s/m^2
ξ	Dynamic peak pressure ratio (ratio of dimensionless dynamic to steady state peak pressure, $P_{max}/(P_{max})\ q = 0$
ω	Circular frequency of harmonic oscillation

INTRODUCTION

Hydrodynamic lubrication of rigid line and point contacts has attracted the attention of tribologists for the past two decades because of its practical applications in the lubrication of lightly loaded rolling-element bearings. The major focus has been in estimating the minimum film thickness and in obtaining a relationship between film thickness, load, and entraining velocity parameters. An early theoretical approach to the hydrodynamic lubrication of rigid cylinders for an incompressible, isoviscous lubricant was presented by

Martin (1916). A classical analytical solution for rigid spherical contacts using half-Sommerfeld boundary conditions for the film rupture was obtained by Kapitsa (1955). Experimental measurements of the film thickness in hydrodynamically lubricated point contacts were reported by Dalmaz and Godet (1974) and Thorp and Gohar (1972). Brewe et al. (1979) obtained a film thickness equation for the lubrication of fully flooded, rigid, isoviscous point contacts through a numerical analysis that used a more realistic Reynolds boundary condition for the film rupture in the exit region. They showed that the film rupture boundary condition resulted in an additional geometry parameter in the film thickness equation. Inlet starvation effects have also been investigated by several researchers, viz Chiu (1974), Dowson (1968), Floberg (1965, 1973), and Wedeven et al. (1971). More recently inlet starvation effects were incorporated into the film thickness equation by Brewe and Hamrock (1982).

Sasaki et al. (1962) presented a solution for the isothermal lubrication of rigid cylinders subjected to sinusoidal load for a non-Newtonian fluid by using superposition of pressure curves generated by normal approach and entraining velocities. Appropriate boundary conditions for the film rupture in the exit were not satisfied. Vichard (1971) analyzed theoretically the transient effect associated with squeeze film action under both hydrodynamic and elastohydrodynamic conditions. He concluded that at low film thickness the damping phenomenon associated with normal approach was more important under elastohydrodynamic conditions than under hydrodynamic conditions. Investigations of the elastohydrodynamic theory of concentrated contacts in normal approach were carried out by Herrebrugh (1970), Christensen (1962), and Lee and Cheng (1973), and more recently by Wang and Cheng (1981) and Chandra and Rogers (1983).

Dowson, Markho, and Jones (1976) presented a general theoretical analysis of the hydrodynamic lubrication of rigid cylindrical contacts by an isoviscous lubricant in combined rolling and normal motion. Results showed that normal motion significantly influences the load-carrying capacity of the contact. The film rupture boundary was also observed to be affected significantly by normal motion. Experimental investigations were also reported by Markho and Dowson (1976). However, a similar theoretical analysis does not exist that incorporates the geometry effect into the hydrodynamic lubrication of rigid point contacts by an isoviscous, incompressible lubricant in combined rolling and normal motion. The present investigation deals with this problem. Through a numerical analysis the effect of squeeze film action due to normal motion combined with entraining action due to pure rolling has been investigated for rigid point contacts. Geometry effects have also been incorporated. Computer plots of pressure distribution depict the effect of normal motion on the pressure distribution and film rupture boundary in the exit region. Sixty-three cases were used to derive an empirical formula for the dynamic load-carrying capacity as a function of the dimensionless normal velocity and geometry parameters. The dynamic peak pressure ratio is also given by a simple formula as a function of these parameters.

THEORETICAL ANALYSIS

Reynolds Equation

The Reynolds equation for the hydrodynamic lubrication of two rigid solids separated by an incompressible, isoviscous lubricant film is given as Eq. (1). Lubricant flow for a rolling-sliding contact and the corresponding pressure buildup is shown in Fig. 1.

$$\frac{\partial}{\partial x}\left(h^3 \frac{\partial p}{\partial x}\right) + \frac{\partial}{\partial y}\left(h^3 \frac{\partial p}{\partial y}\right) = 12\eta_0 U_S \left(\frac{\partial h}{\partial x}\right) + 12\eta_0 U_N \qquad (1)$$

where

$$\left.\begin{aligned} X &= x/R_x;\ Y = y/R_x;\ H = h/R_x;\ P = pR\mu/\eta_0 U_S;\ \alpha = R_y/R_x; \\ U_S &= 1/2\ (U_A + U_B);\ \bar{U}_N = U_N/U_S \end{aligned}\right\} \quad (2)$$

Eq. (1) can then be expressed in dimensionless form as

$$\frac{\partial}{\partial X}\left(H^3 \frac{\partial P}{\partial X}\right) + \frac{\partial}{\partial X}\left(H^3 \frac{\partial P}{\partial X}\right) = 12 \left(\frac{\partial H}{\partial X}\right) + \bar{U}_N \quad (3)$$

Eq. (3) can be rewritten as

$$\frac{\partial}{\partial X}\left(H^3 \frac{\partial P}{\partial X}\right) + \frac{\partial}{\partial Y}\left(H^3 \frac{\partial P}{\partial Y}\right) = 12 \left(\frac{\partial H}{\partial X} + \sqrt{2H_0}\, q\right) \quad (4)$$

where $q = \bar{U}_N/\sqrt{2H_0}$ is the dimensionless normal velocity parameter that incorporates the dimensionless normal velocity $\bar{U}_N$ and the central film thickness H_0.

The boundary conditions for Eq. (4) are given as

$$\left.\begin{aligned} &P = 0 \text{ at the inlet boundary (i.e., } H = H_{in}) \\ &P = \frac{\partial P}{\partial N} = 0 \text{ at the cavitation boundary (i.e., Reynolds boundary condition), where } N \text{ is the normal to the boundary.} \end{aligned}\right\} \quad (5)$$

Film Shape

The thickness of a hydrodynamic film between two rigid bodies in rolling contact can be written as the sum of two terms, that is,

$$h = h_0 + S(x,y) \quad (6)$$

where

h_0 Central (or minimum) film thickness

$S(x,y)$ Separation due to geometry of solids

The separation of two rigid solids is shown in Fig. 2. The film shape can be expressed in dimensionless form by following the widely used parabolic approximation as

$$H = H_0 + \frac{X^2}{2} + \frac{Y^2}{2\alpha} \tag{7}$$

The dimensionless parameters involved in the subsequent numerical investigation are therefore the central film thickness H_0, the normal velocity parameter q, and the geometry parameter α.

A pressure distribution satisfying the Reynolds equation (Eq. (4)) and the boundary conditions given by Eq. (5) was determined for a given speed, viscosity, central film thickness, fluid inlet level, and normal velocity parameter by using the Gauss-Seidel iterative method with overrelaxation. For optimum efficiency nonuniform nodal structure consisting of coarse and fine mesh was used to enhance accuracy in the region of high pressure and large pressure gradients.

A fine mesh spacing of 0.001 and a coarse mesh spacing of 0.01 were used in all of the cases run for $\alpha = 1.0$. For geometry parameters other than $\alpha = 1.0$ boundaries of the computation zone were located according to the relationship $Y = \alpha^{0.5}X$ and correspondingly coarser grids in the Y direction were used for higher values of α. Grid sizes were varied until no appreciable influence on the pressure distribution or the load-carrying capacity was found.

Hydrodyanmic Load-Carrying Capacity

The load-carrying capacity can be calculated by integrating the pressure in the contact region and is written as

$$w = \int_A p \, dxdy \tag{8}$$

In dimensionless form it is expressed as

$$W = w/\eta_0 U_S R_x = \int_A P \, dxdy \tag{9}$$

where A is the domain of integration that is dependent both on the fluid inlet level and the cavitation boundary.

Instantaneous load-carrying capacity is expressed as a ratio:

$$\beta = \frac{W}{(W)q} \geq 0.0 \tag{10}$$

$(W)q = 0$ represents the dimensionless steady state value of w evaluated for the same operating conditions and the same minimum film thickness.

RESULTS AND DISCUSSION

Results of numerical calculations that show the steady state performance of typical nonconformal contacts are presented in Tables 1 and 2, showing, respectively, the effects of the parameters H_0 and α.

The dynamic performance of hydrodynamically lubricated nonconformal contacts in combined rolling and normal motion is governed by the dimensionless normal velocity parameter q. It incorporates three major parameters, viz normal velocity, entraining velocity, and central film thickness. Representative results for dynamic load ratio β, dynamic peak pressure ratio ξ, and the dimensionless locations of the peak pressure X_p and the film rupture boundary X_r are presented in Table 3 for a fixed value of dimensionless central film thickness $H_0 = 1.0 \times 10^{-3}$ and with dimensionless normal velocity parameter q varying between -1.0 and 0.75. In Tables 4 and 5 similarly, H_0 assumes the fixed values 1×10^{-4} and 1×10^{-5}, respectively. The dynamic load ratios of Table 4 are also displayed graphically in Fig. 3. The normal velocity parameter q clearly has a significant pressure-generating effect during normal approach and thereby increases the dynamic load ratio β

with increasing normal velocity parameter. On the contrary, β was significantly reduced during normal separation for $q > 0$.

The magnitude of the peak pressure generated in a contact, its location, and the location of the film rupture boundary are also affected significantly by the normal velocity. Pressure distributions for various values of the normal velocity parameter taken from Table 4 are shown in Fig. 4. The inlet meniscus boundary is not shown in these figures. During normal approach the film rupture boundary moves downstream into the exit region (or the divergent portion of the film) with reference to the minimum-film-thickness position. During separation it moves upstream, reaching the convergent portion of the film for higher values of normal velocity parameter. Similar observations were made by Dowson et al. (1976) for the lubrication of rigid cylinders in combined rolling and normal motion. The location of the pressure peak and the entire pressure distribution in the contact also shift accordingly. Thus superposition of normal motion on the entraining velocity alters both the magnitude and distribution of the pressure in the contact.

Variation of peak pressure ratio ξ is shown in Fig. 5, again for data from Table 4. Pressures of the order of 3 to 4 times the corresponding peak pressure in the steady state situation are generated in the contact during normal approach. Relative reductions in the peak pressures of similar magnitude occur during separation.

The influence of the geometry parameter α on the dynamic load ratio β and the peak pressure ratio ξ is shown in Table 6 and in Figs. 6 and 7, respectively. Recall that for $\alpha > 1$ the major axis of the film contours is transverse to the entrainment velocity, so for $\alpha >> 1$ the geometry resembles the usual case of a lubricated cylinder. During normal approach β increases with increase in α up to a certain value and then it tends to approach a

limiting value for further increase in α. Similarly, during separation, the β initially decreases with increasing α and then approaches a limiting value for higher values of α. Similar variations with x are observed for the dynamic peak pressure ratio ξ. Therefore it can be said that α significantly affects the dynamic performance of nonconformal contacts for values of α within the practically useful range 0.2 to 10. However, for α between 10 and 35 the geometry parameter effects are small. For most practical situations the values of q and H_0 fall within the ranges considered in the present calculations. For the sixty-three cases run β can be expressed as a function of q and α by a simple formula for the complete range of data presented in the Tables 3 to 6 as follows:

$$\beta = \left\{\alpha^{-0.028} \operatorname{sech}\,(1.68\,q)\right\}^{1/q} \qquad \text{for } q \neq 0 \tag{11}$$

Note that Eq. (11) does not explicitly contain the central film thickness parameter H_0 for the following reason: While H_0 appears both in the Reynolds equation and in the parameter q, comparison of Tables 3 to 5 reveals only a very minor explicit dependence of β upon H_0. For ξ this dependence is still less. It is therefore sufficiently accurate, except perhaps for larger negative q, to use values averaged with respect to H_0 in deriving a relationship such as presented in Eq. (11).

The dynamic load ratio for rigid point contacts undergoing harmonic oscillations can also be determined by using Eq. (11). For small-amplitude oscillations about the mean film thickness, the parameter q oscillates with amplitude q_{max} given by

$$q_{max} = \frac{R_x}{2U_s}\sqrt{2(H_0)_{mean}}\,\omega\varepsilon \tag{12}$$

Since a negative q enhances the dynamic load ratio more than a positive q diminishes it, such oscillations must generate a higher average load-carrying capacity.

It has been mentioned that significantly higher peak pressures can be generated in the contact during normal approach than during normal separation. Therefore the estimation of peak pressures in the contact is of practical importance for estimating the maximum stress in the contact and the fatigue life of the contact. Dynamic peak pressure ratio ξ is expressed by a simple formula as a function of the normal velocity parameter q and the geometry parameter α

$$\xi = \left\{\alpha^{-0.032} \text{ sech } (2q)\right\}^{1/q} \quad \text{for } q \neq 0.0 \tag{13}$$

Eqs. (11) and (13) are valid for the complete range of α between 0.2 and 35.

Tables 7 to 8 show the percentage error between the values obtained from the preceding formulas and the computed values for both dynamic load ratio and peak pressure ratio. In general the agreement is excellent, and the formulas should find a good practical application. The slight explicit dependence of β upon H_0 has not been incorporated into the present formulas.

The present formulas give excellent correlation for the dynamic peak pressure ratio ξ during normal approach. However, correlation does not appear good for higher values of q during separation. During separation for higher values of q (e.g., 0.5 and 0.75) the rupture boundary moves into the convergent portion of the fluid film and thereby shifts the pressure peak and the entire pressure distribution from the central film thickness into the inlet region. This alters the physical situation in the contact and perhaps warrants a closer look than was intended here. Rupture of the fluid film in the inlet region might lead to the failure of the lubrication process in the contact under certain situations.

CONCLUSIONS

A numerical solution to the hydrodynamic lubrication of nonconformal rigid contacts with an incompressible, isoviscous lubricant in combined rolling and normal motion has been obtained. The following conclusions were reached through a parametric study:

1. Normal motion combined with pure rolling motion significantly increases load-carrying capacity and peak pressure in the contact during normal approach. A correspondingly significant decrease in load-carrying capacity and peak pressure occurs during normal separation.

2. The film rupture (or cavitation) boundary moves further into the exit region away from the minimum-film-thickness position during normal approach but moves toward the inlet and into the convergent portion of the film for higher normal velocities during separation.

3. Increasing the geometry parameter increases dynamic load-carrying capacity and peak pressure during normal approach. Reverse effects are observed during separation.

4. The dynamic load ratio β and the dynamic peak pressure ratio ξ are very weakly dependent on central film thickness and can be adequately expressed in terms of the dimensionless normal velocity parameter q and the geometry parameter α by simple equations as follows:

$$\beta = \left\{\alpha^{-0.028}\ \text{sech}\ (1.68\ q)\right\}^{1/q}$$

$$\xi = \left\{\alpha^{-0.032}\ \text{sech}\ (2q)\right\}^{1/q}$$

REFERENCES

Brewe, D. E., Hamrock, B. J., and Taylor, C. M., "Effect of Geometry on Hydrodynamic Film Thickness," Journal of Lubrication Technology, Vol. 101, No. 2, Apr. 1979, pp. 231-239.

Brewe, D. E. and Hamrock, B. J., "Analysis of Starvation Effects on Hydrodynamic Lubrication in Nonconforming Contacts," Journal of Lubrication Technology, Vol. 104, No. 3, July 1982, pp. 410-417.

Chandra, A. and Rogers, R. J., "The Normal Approach, Contact, and Rebound of Lubricated Cylinders," Journal of Lubrication Technology, Vol. 105, No. 2, Apr. 1983, pp. 271-279.

Chiu, Y. P., "An Analysis and Prediction of Lubricant Film Starvation in Rolling Contact Systems," ASLE Transactions, Vol. 17, No. 1, 1974, pp. 22-35.

Christensen, H., "The Oil Film in a Closing Gap," Proceedings of the Royal Society of London, Series A. Mathematical and Physical Sciences, Vol. 266, No. 1326, 20 Mar. 1962, pp. 312-328.

Dalmaz, G. and Godet, M., "Traction, Load and Film Thickness in Lightly-Loaded Lubricated Point Contacts," Journal of Mechanical Engineering Science, Vol. 15, No. 6, Dec. 1973, pp. 400-409.

Dalmaz, G. and Godet, M., "Effebs des Conditions d'Alimentation Sur l'Epaisseur du Film daus les Contacts Hertziens Lubrifies Mec. Materiaux Elec. (France) no. 296-297, Aug. to Sept. 1974, pp. 25-34 (see NASA TM-75782, 1980, for transl.).

Dowson, D., "Laboratory Experiments and Demonstrations in Tribology," Tribology, Vol. 1, No. 2, Mar. 1968, pp. 104-108; and Vol. 1, No. 3, Aug. 1968, pp. 150-156.

Dowson, D., Markho, P. H., and Jones, D. A., "The Lubrication of Lightly Loaded Cylinders in Combined Rolling, Sliding, and Normal Motion. Part I: Theory," Journal of Lubrication Technology, Vol. 98, No. 4, Oct. 1976, pp. 509-516.

Floberg, L., "On Hydrodynamic Lubrication with Special Reference to Sub-cavity Pressures and Number of Streamers in Cavitation Regions," Acta Polytechnica Scandinavica (Mechanical Engineering Series), No. 19, 1965, pp. 1-35.

Floberg, L., "Lubrication of Two Rotating Cylinders at Variable Lubricant Supply with Reference to the Tensile Strength of the Liquid Lubricant," Journal of Lubrication Technology, Vol. 95, No. 2, Apr. 1973, pp. 155-165.

Herrebrugh, K., "Elastohydrodynamic Squeeze Films Between Two Cylinders in Normal Approach," Journal of Lubrication Technology, Vol. 92, No. 2, Apr. 1970, pp. 292-302.

Kapitsa, P. L., "Hydrodynamic Theory of Lubrication During Rolling Friction," Zhurnal Tekhnicheskoi Fiziki, Vol. 25, No. 4, 1955, pp. 747-762.

Lee, K. M. and Cheng, H. S., "The Pressure and Deformation Profiles Between Two Normally Approaching Lubricated Cylinders," Journal of Lubrication Technology, Vol. 95, No. 3, July 1973, pp. 308-320.

Markho, P. H. and Dowson, D., "The Lubrication of Lightly Loaded Cylinders in Combined Rolling, Sliding and Normal Motion. Part II: Experimental," Journal of Lubrication Technology, Vol. 98, No. 4, Oct. 1976, pp. 517-523.

Martin, H. M., "Lubrication of Gear Teeth," Engineering, (London), Vol. 102, Aug. 11, 1916, pp. 119-121.

Sasaki, T., Mori, H., and Okino, N., "Fluid Lubrication Theory of Roller Bearing, Part I: Fluid Lubrication Theory for Two Rotating Cylinders in Contact," Journal of Basic Engineering, Vol. 84, No. 1, pp. 166-174; "Part II: Fluid Lubrication Theory Applied to Roller Bearing," Journal of Basic Engineering, Vol. 84, No. 1, Mar. 1962, pp. 175-180.

Thorp N. and Gohar, R., "Oil Film Thickness and Shape for a Ball Sliding in a Grooved Raceway," Journal of Lubrication Technology, Vol. 94, No. 3, July 1972, pp. 199-210.

Vichard, J.P., "Transient Effects in the Lubrication of Hertzian Contacts," Journal of Mechanical Engineering Science, Vol. 13, No. 3, June 1971, pp. 173-189.

Wang, K. L. and Cheng, H. S., "A Numerical Solution to the Dynamic Load, Film Thickness, and Surface Temperatures in Spur Gears, Part 1: Analysis," Journal of Mechanical Design, Vol. 103, No. 1, Jan. 1981, pp. 177-187.

Wedeven, L. D., Evans, D., and Cameron, A., "Optical Analysis of Ball Bearing Starvation," Journal of Lubrication Technology, Vol. 93, No. 3, July 1971, pp. 349-363.

TABLE 1. - STEADY STATE PERFORMANCE OF NONCONFORMAL CONTACTS - EFFECT OF MINIMUM FILM THICKNESS

[Geometry parameter $\alpha = 1.0$; inlet starvation parameter $H_{in} = 0.035$; dimensionless normal velocity parameter $q = 0.0$]

Dimensionless minimum film thickness, H_0	Dimensionless load-carrying capacity, W	Dimensionless peak pressure, P_{max}	Dimensionless location of peak pressure,[a] X_p	Dimensionless location of film rupture boundary,[a] X_r
1.0×10^{-3}	270.8	3.77655×10^{4}	-0.023	+0.015
1.0×10^{-4}	1061.2	1.2105×10^{6}	-.007	+.005
1.0×10^{-5}	3493.76	3.8246×10^{7}	-.002	+.002

[a](-) indicates location toward inlet side with respect to minimum-film-thickness position; (+) indicates location toward exit side.

TABLE 2. - STEADY STATE PERFORMANCE OF NONCONFORMAL CONTACTS - EFFECT OF GEOMETRY

[Dimensionless minimum film thickness $H_0 = 1.0\times10^{-4}$; inlet starvation parameter $H_{in} = 0.035$; normal velocity parameter $q = 0.0$.]

Geometry parameter, α	Dimensionless load-carrying capacity, W	Dimensionless peak pressure, P_{max}	Dimensionless location of peak pressure,[a] X_p	Dimensionless location of film rupture boundary,[a] X_r
0.2	171.0	0.4298×10^{6}	-0.008	+0.003
.4	404.1	$.7173\times10^{6}$	-.008	+.004
.6	633.1	$.9217\times10^{6}$	-.007	+.004
.8	852.4	1.0766×10^{6}	↓	+.005
1.0	1061.2	1.2105×10^{6}		+.005
2.0	1905.4	1.5377×10^{6}		+.006
5.0	3660.0	1.8479×10^{6}		+.006
10.0	5646.6	1.9958×10^{6}		+.006
20.0	8168.3	2.0498×10^{6}		+.007
35.0	10987.2	2.0820×10^{6}	↓	+.007

[a](-) indicates location toward inlet side with respect to minimum-film-thickness position; (+) indicates location toward exit side.

TABLE 3. - DYNAMIC PERFORMANCE OF NONCONFORMAL CONTACTS - EFFECT OF DIMENSIONLESS NORMAL VELOCITY PARAMETER

[Dimensionless minimum film thickness $H_0 = 1.0 \times 10^{-3}$; geometry parameter $\alpha = 1.0$; inlet starvation parameter $H_{in} = 0.035$.]

Dimensionless normal velocity parameter,[a] q	Dynamic load ratio, β	Dynamic peak pressure ratio, ξ	Dimensionless location of peak pressure,[a] X_p	Dimensionless location of film rupture boundary,[a] X_r
-1.0	2.98	3.7408	-0.008	+0.043
-.75	2.316	2.9258	-.010	+.036
-.5	1.859	2.2166	-.013	+.033
-.25	1.403	1.5531	-.017	+.029
-.1	1.15	1.2034	-.020	+.021
-.05	1.073	1.0984	-.022	+.018
+.05	.931	.9076	-.025	+.013
+.1	.866	.8223	-.026	+.010
+.25	.695	.6161	-.031	+.003
+.5	.479	.3460	-.044	-.010
+.75	.332	.2017	-.054	-.020

[a](-) indicates location toward inlet side with respect to minimum-film-thickness position; (+) indicates location toward exit side.

TABLE 4. - DYNAMIC PERFORMANCE OF NONCONFORMAL CONTACTS - EFFECT OF DIMENSIONLESS NORMAL VELOCITY PARAMETER

[Dimensionless minimum film thickness $H_0 = 1.0 \times 10^{-4}$; geometry parameter $\alpha = 1.0$; inlet starvation parameter $H_{in} = 0.035$.]

Dimensionless normal velocity parameter,[a] q	Dynamic load ratio, β	Dynamic peak pressure ratio, ξ	Dimensionless location of peak pressure,[a] X_p	Dimensionless location of film rupture boundary,[a] X_r
-1.0	2.783	3.79	-0.003	+0.024
-.75	2.258	3.0143	-.003	+.019
-.5	1.774	2.2486	-.004	+.014
-.25	1.348	1.56	-.005	+.009
-.1	1.129	1.2053	-.006	+.008
-.05	1.063	1.1002	-.007	+.006
+.05	.941	.906	-.008	+.004
+.1	.885	.8195	-.008	+.003
+.25	.738	.5981	-.010	+.001
+.5	.553	.3462	-.013	-.003
+.75	.422	.2039	-.017	-.006

[a](-) indicates location toward inlet side with respect to minimum-film-thickness position; (+) indicates location toward exit side.

TABLE 5. - DYNAMIC PERFORMANCE OF NONCONFORMAL CONTACTS - EFFECT OF DIMENSIONLESS NORMAL VELOCITY PARAMETER

[Dimensionless minimum film thickness $H_0 = 1.0 \times 10^{-5}$; geometry parameter $\alpha = 1.0$; inlet starvation parameter $H_{in} = 0.035$.]

Dimensionless normal velocity parameter, q	Dynamic load ratio, β	Dynamic peak pressure ratio, ξ	Dimensionless location of peak pressure,[a] X_p	Dimensionless location of film rupture boundary,[a] X_r
-1.0	2.62	3.7588	-0.001	+0.007
-.75	2.147	2.9831	-.001	+.006
-.5	1.71	2.2184	-.001	+.004
-.25	1.321	1.5382	-.002	+.003
-.1	1.12	1.2111	↓	+.002
-.05	1.06	1.1054	↓	+.002
+.05	.944	.8984	↓	+.001
+.1	.894	.8100	-.003	+.001
+.25	.754	.6061	-.003	0
+.5	.578	.3540	-.004	-.001
+.75	.454	.2074	-.005	-.002

[a](-) indicates location toward inlet side with respect to minimum-film-thickness position; (+) indicates location toward exit side.

TABLE 6. - DYNAMIC PERFORMANCE OF NONCONFORMAL CONTACTS - EFFECT OF GEOMETRY PARAMETER

[Dimensionless minimum film thickness $H_0 = 1.0 \times 10^{-4}$; inlet starvation parameter $H_{in} = 0.035$.]

Geometry parameter, α	Dimensionless normal velocity parameter,[a]							
	q = -1.0				q = +0.75			
	Dynamic load ratio, β	Dynamic peak pressure ratio, ξ	Dimensionless location of peak pressure,[a] X_p	Dimensionless location of film rupture boundary,[a] X_r	Dynamic load ratio, β	Dynamic peak pressure ratio, ξ	Dimensionless location of peak pressure,[a] X_p	Dimensionless location of film rupture boundary,[a] X_r
0.2	2.5971	3.5697	-0.003	+0.019	0.4485	0.2232	-0.017	-0.007
.4	2.6684	3.6646	↓	+.021	.4370	.2148	↓	- .007
.6	2.7195	3.7289	↓	+.023	.4299	.2101	↓	-0.006
.8	2.7533	3.7704	↓	+.024	.4253	.2063	↓	↓
1.0	2.7830	3.7900	↓	+.024	.4220	.2039	↓	↓
2.0	2.8594	3.9227	-.002	+.026	.4121	.1951	-0.016	↓
5.0	2.9380	4.0505	↓	+.028	.4032	.1879	↓	-0.005
10.0	2.9770	4.1242	↓	+.029	.3970	.1840	↓	↓
20.0	2.9848	4.1497	↓	+.029	.3969	.1829	↓	↓
35.0	2.9931	4.1668	↓	+.029	.3966	.1821	↓	↓

TABLE 7. - PERCENTAGE ERROR BETWEEN VALUES OF DYNAMIC LOAD RATIO AND PEAK PRESSURE RATIO GIVEN BY FORMULAS AND NUMERICALLY CALCULATED VALUES FOR VARIOUS DIMENSIONLESS NORMAL VELOCITY PARAMETERS

Dimensionless normal velocity parameter,[a] q	Central film thickness, H_0					
	$1.0x10^{-3}$	$1.0x10^{-4}$	$1.0x10^{-5}$	$1.0x10^{-3}$	$1.0x10^{-4}$	$1.0x10^{-5}$
	Percentage of error in dynamic load ratio β			Percentage error in dynamic pressure ratio ζ		
-1.0	7.35	-0.25	-5.95	0.57	-0.73	0.09
-.75	1.93	4.55	9.96	6.93	3.79	4.88
-.50	1.56	6.43	10.41	7.42	5.89	7.33
-.25	.43	4.53	6.66	4.10	3.64	5.11
-.10	.07	1.93	2.75	1.36	1.20	.72
-.05	0	.94	1.23	.60	.44	-.04
+.05	.10	-.96	-1.28	-.29	-.11	.73
+.10	.34	-1.81	-2.80	-.30	.04	1.21
+.25	2.12	-3.83	-5.87	.39	3.43	2.05
+.50	-8.36	-4.22	10.58	21.38	21.31	18.64
+.75	21.70	.47	-7.1	58.65	56.76	54.29

[a](-) indicates location toward inlet side with respect to minimum-film-thickness position; (+) indicates location toward exit side.

TABLE 8. - PERCENTAGE ERROR BETWEEN VALUES OF DYNAMIC LOAD RATIO AND PEAK PRESSURE RATIO GIVEN BY FORMULAS AND NUMERICALLY CALCULATED VALUES FOR VARIOUS DIMENSIONLESS GEOMETRY PARAMETERS

Geometry parameter, α	Normal approach (q = -1.0)	Separation (q = 0.75)	Normal approach (q = -1.0)	Separation (q = 0.75)
	Percentage error in dynamic ratio β		Percentage error in dynamic peak pressure ratio ζ	
0.2	2.18	0.18	0.10	53.38
.4	1.41	.31	-.30	54.74
.6	.61	.41	-.74	55.49
.8	.21	.50	-.93	56.42
1.0	-.25	.38	-.73	56.76
2.0	-1.00	.19	-1.94	59.06
5.0	-1.16	-1.02	-2.21	58.82
10.0	-.54	-2.09	-1.80	57.46
20.0	1.13	-4.59	-.22	53.79
35.0	2.46	-6.57	1.17	50.82

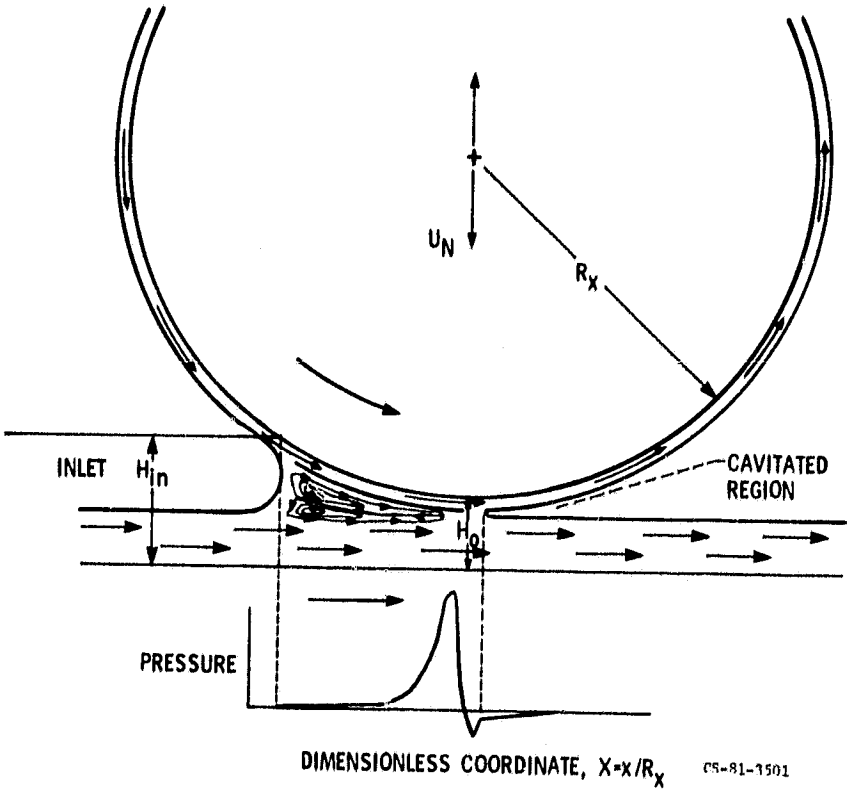

Fig. 1. - Depiction of lubricant flow for a rolling-sliding contact and corresponding pressure buildup.

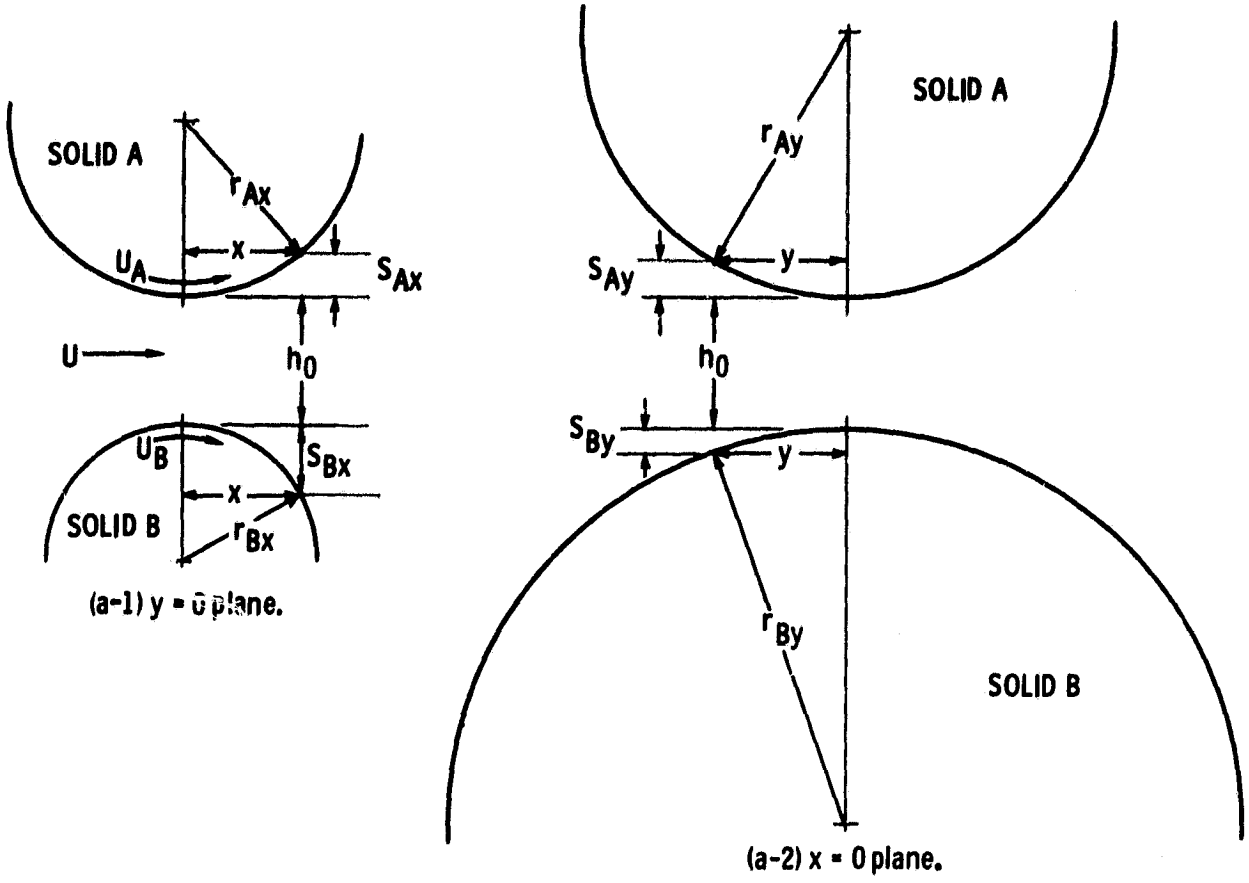

(a-1) y = 0 plane.

(a-2) x = 0 plane.

(a) Two rigid solids separated by a lubricant film.

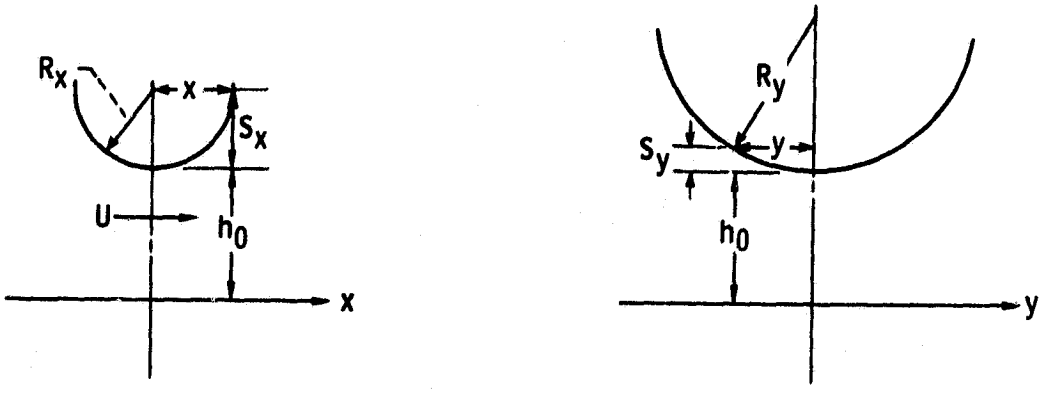

(b-1) y = 0 plane

(b-2) x = 0 plane.

(b) Equivalent system of a rigid solid near a plane separated by a lubricant film.

Fig. 2 - Contact geometry.

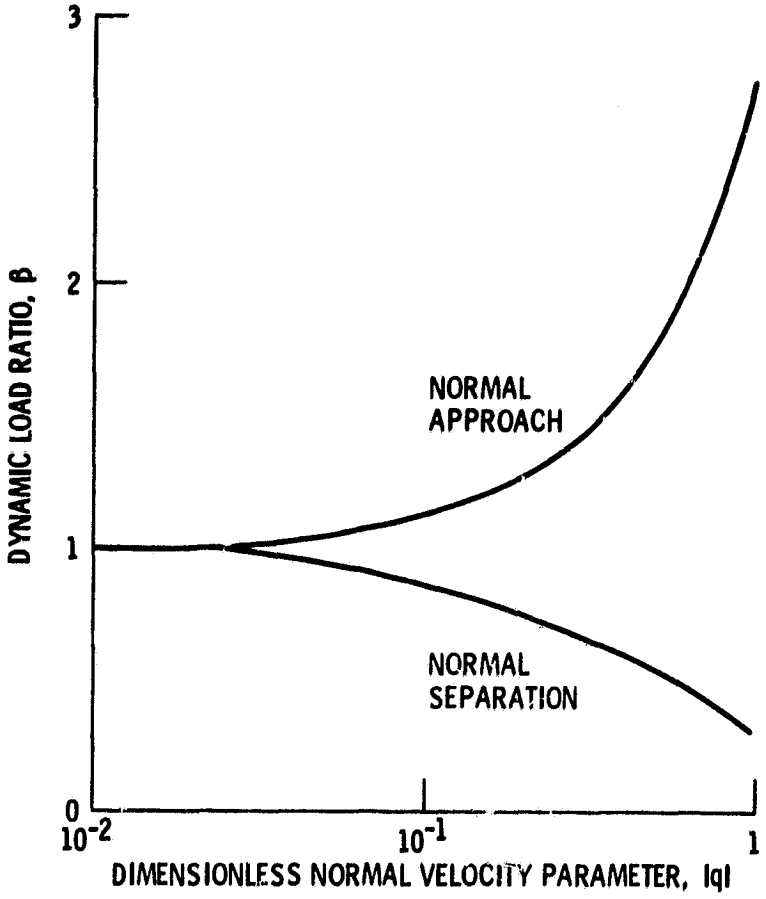

Fig. 3. - Variation of dynamic load ratio with dimensionless normal velocity parameter. Dimensionless central film thickness $H_0 = 1.0 \times 10^{-4}$; dimensionless geometry parameter $\alpha = 1.0$; and dimensionless inlet starvation parameter $H_{in} = 0.035$.

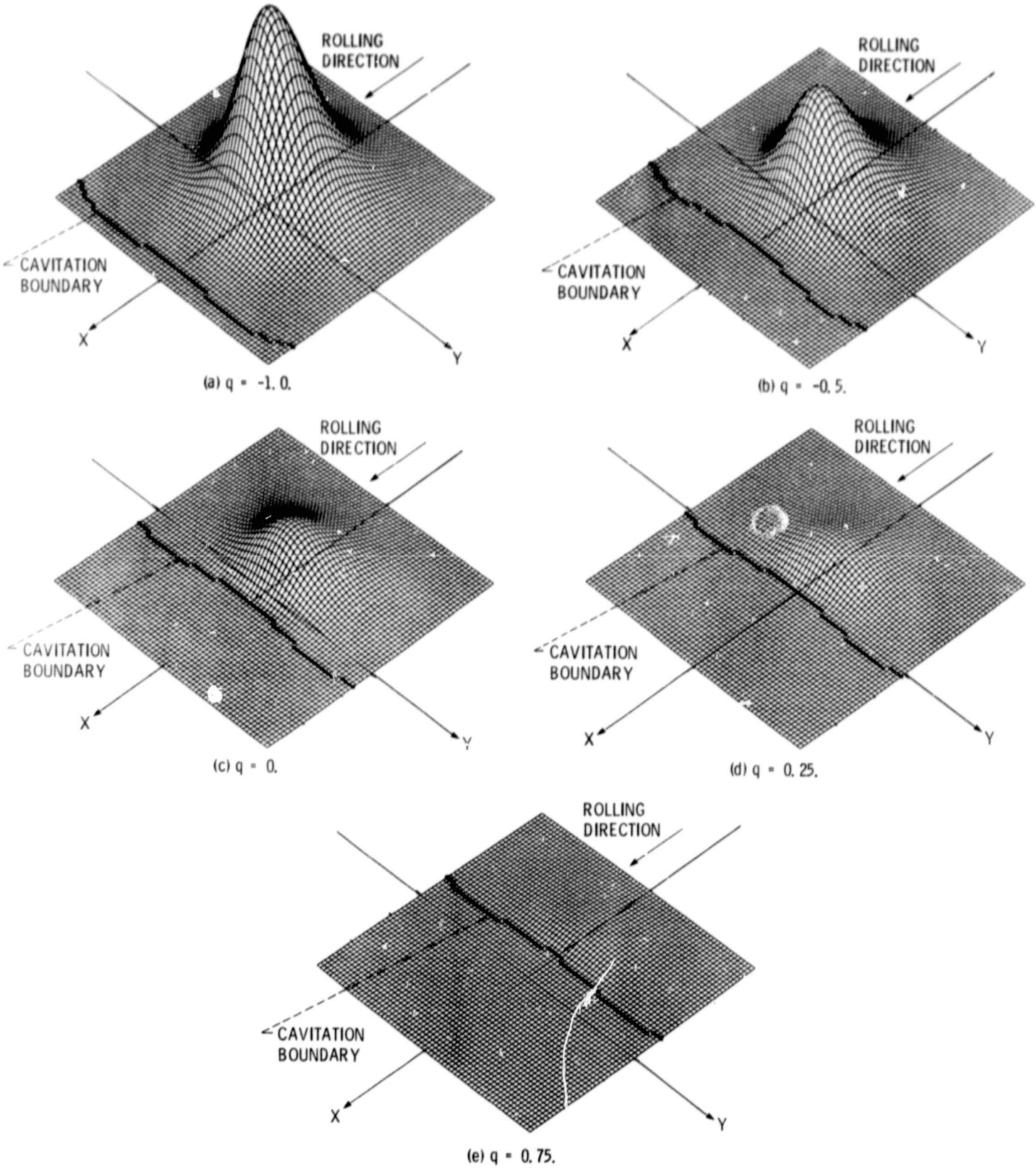

Fig. 4. - Pressure distribution in contact for various values of dimensionless normal velocity parameter q. Dimensionless central film thickness $H_0 = 1.0 \times 10^{-4}$; dimensionless geometry parameter $\alpha = 1.0$; and dimensionless inlet starvation parameter $H_{in} = 0.0006$.

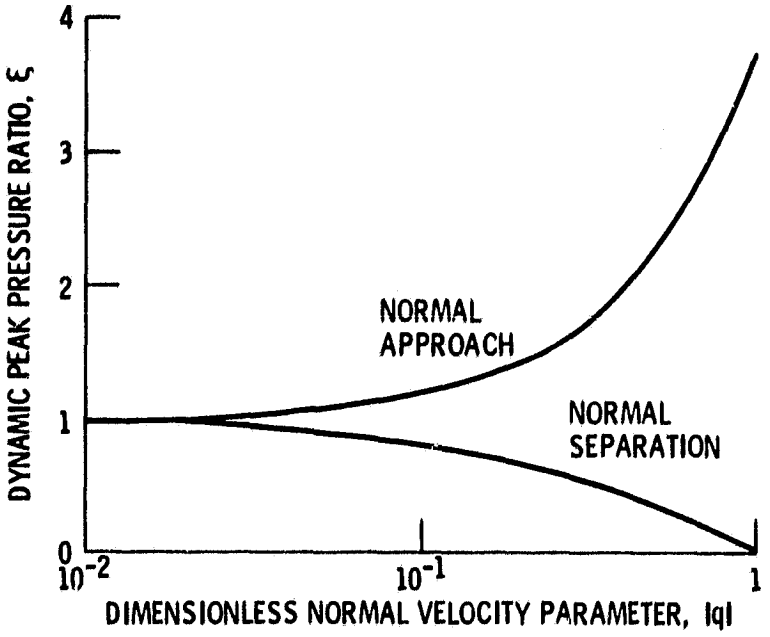

Fig. 5. - Variation of dynamic peak pressure ratio with dimensionless normal velocity parameter. Dimensionless central film thickness $H_0 = 1.0 \times 10^{-4}$; dimensionless geometry parameter $\alpha = 1.0$; and dimensionless inlet starvation parameter $H_{in} = 0.035$.

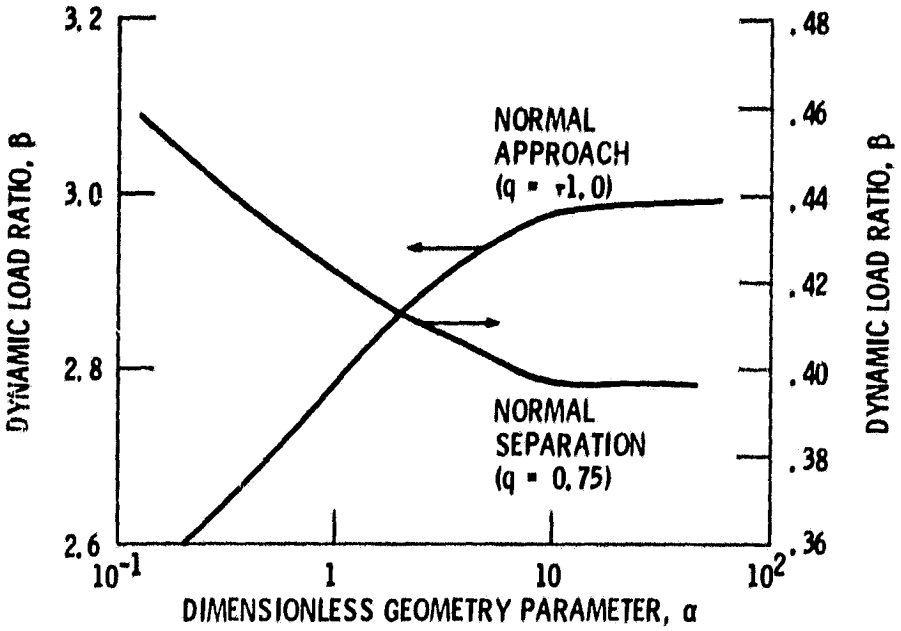

Fig. 6. - Variation of dynamic load ratio with dimensionless geometry parameter. Dimensionless central film thickness $H_0 = 1.0 \times 10^{-4}$; and dimensionless inlet starvation parameter $H_{in} = 0.035$.

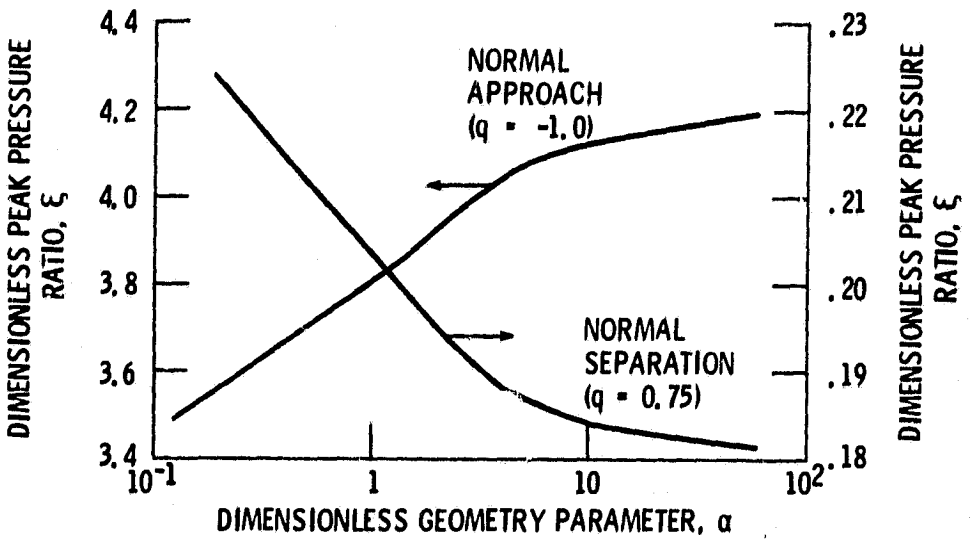

Fig. 7. - Variation of dynamic peak pressure ratio with dimensionless geometry parameter. Dimensionless central film thickness $H_0 = 1.0 \times 10^{-4}$; and dimensionless inlet starvation parameter $H_{in} = 0.035$.